Manuscript

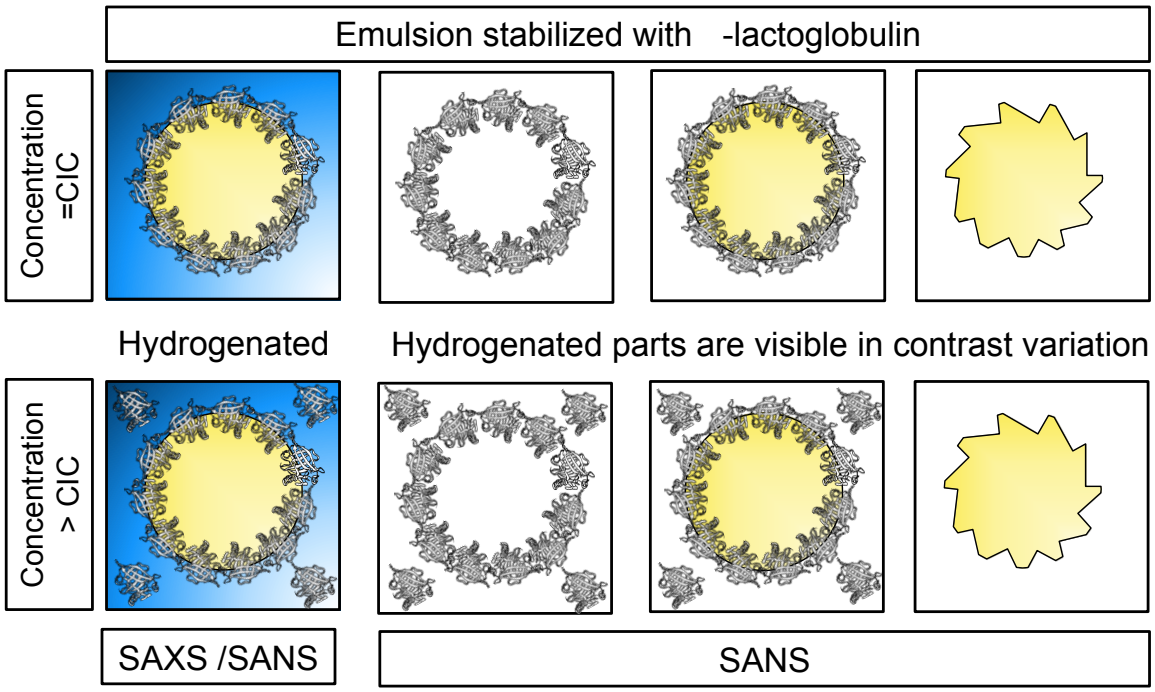


Graphical abstract

# New insights into protein stabilized emulsions captured via neutron and X-ray scattering: An approach with β-lactoglobulin at triacylglyceride-oil/water interfaces

Theresia Heiden-Hecht*[1], Baohu Wu[1], Kuno Schwärzer[2], Stephan Förster[1,2], Joachim Kohlbrecher[3], Olaf Holderer[1] and Henrich Frielinghaus[1]

[1] Jülich Centre for Neutron Science (JCNS) at Heinz Maier-Leibnitz Zentrum (MLZ), Forschungszentrum Jülich GmbH, Lichtenbergstr. 1, 85747 Garching, Germany

[2] Jülich Centre for Neutron Science (JCNS-1), Forschungszentrum Jülich GmbH, 52425 Jülich, Germany

[3] Paul Scherrer Institut, Villingen 5232, Switzerland

*Corresponding author: E-mail-address: t.heiden-hecht@fz-juelich.de, telephone-number: 004989158860841

## Abstract

**Hypothesis:** To analyze protein stabilized emulsions, SAXS and SANS are emerging techniques capturing oil droplet radius, interfacial coverage and structure. Protein shape, thus protein structure change during interfacial adsorption with partial protein unfolding is detected via SAXS analysis at and below the monolayer concentration for proteins, known as critical interfacial concentration (CIC). SANS determines the same phenomena below and above the CIC, via contrast variation and coarse-grained modelling.

**Experiments:** β-lactoglobulin concentration dependent SAXS experiments were performed focusing on molecular length scales to characterize protein shape in water, and interfacial structure in emulsions. Complementary SANS experiments with contrast variation via deuterated triacylglyceride-oil provided insight into oil droplet radius, interfacial coverage and structure via data analysis with scattering models and low-resolution shape reconstruction with the DENFERT model.

**Findings:** SAXS and SANS experiments allowed to determine the interfacial structure below and above the CIC, as well as oil droplet radius and interfacial coverage. These findings were identified via $Q^{-4}$ Porod scattering at low-Q, protein scattering at high Q, and a $Q^{-2}$ scattering of the interface. Since SANS with accurate contrast variation highlights the interface in comparison to other techniques like FTIR, the presented results show a high impact to understand interfaces in emulsions.

## Highlights

- SANS and SAXS improve understanding of protein stabilized emulsions.
- Oil droplet radius, interfacial coverage and interfacial protein structure are determined.
- Via SAXS change in interfacial protein structure below CIC is detectable.
- Via SANS and contrast variation change in interfacial protein structure above CIC is shown.
- For SANS, coarse grained modelling clarifies change in protein shape.

## Keywords

Emulsions, oil/water interfaces, β-lactoglobulin, SANS, SAXS, DENFERT, contrast variation, scattering, food emulsions, proteins

## 1.Introduction

Emulsions are biphasic and often thermodynamically unstable systems, which are stabilized by amphiphilic components like proteins [1–4]. Protein-stabilized emulsions are widely used in food, cosmetic and pharmaceutical applications due to their ability to improve texture, stability and shelf-life. Important characteristics of emulsions are captured by the oil droplet size, and the interfacial properties [1,2,4]. For proteins, the interfacial properties include: the migration to the interface, the adsorption at the interface, and the resulting interfacial arrangement and unfolding including the interfacial layer thickness, packing and rheology [2,5,6]. These interfacial properties strongly depend -beside other factors- on external parameters like pH or ionic strength, and protein concentration [7–9]. The external parameters determine the protein organization in e.g., dimers or monomers [10–12]. The protein concentration determines the interfacial packing and interfacial unfolding whereby the "critical interfacial concentration" displays the protein concentration to cover the entire oil/water interface with an unfolded protein monolayer [8,9]. Above the CIC it is believed that proteins form multilayers at the oil/water interface [13,14].

Commonly used proteins for emulsion stabilization are whey, casein, soy and egg albumin. These proteins have unique structural and functional properties that allow them to interact with both the oil and water phases of the emulsion, forming an interfacial layer that plays a central role in determining the properties of emulsions [7]. β-Lactoglobulin is a globular protein and the major whey protein used in dairy products. Emulsion systems stabilized with β-lactoglobulin and β-lactoglobulin stabilized oil/water interfaces were extensively studied in all of the

above-mentioned characteristics. Most publications focused on influencing factors like pH, ionic strength and temperature [7,9,15–30], or protein concentration [8,9]. The dimeric organization of β-lactoglobulin at pH 7 affects the interfacial properties, as well as the protein concentration below, at or above the CIC of β-lactoglobulin, which ranges mostly between 0.10 to 0.25%, and sometimes up to 0.35% [8,31,32].

The characteristics of emulsions and interfaces are captured with various methods. Commonly, the oil droplet size is measured via static light scattering [1,2,6,8,22,33–36], or Nuclear Magnetic Resonance [37,38]. The interfacial properties are investigated with a whole range of methods. The migration to the interface, the adsorption at the interface, or the interfacial rheology are often measured via drop tensiometry, additionally via interfacial shear rheology, via *Langmuir* trough or molecular dynamics simulation [22,24,26,29–31,39–42]. The interfacial rearrangement of the protein secondary structure is analyzed via Fourier-Transformation-Infrared-Spectroscopy, Circular Dichroism or Nuclear Magnetic Resonance [8,15–18,21,43]. The interfacial layer thickness is often captured via ellipsometry [44].

More recently, methods like Small-Angle-Neutron-Scattering and Small-Angle-X-ray-Scattering have been used to investigate several of the above-mentioned characteristics at the same time [35,36], techniques, which is in our point of view not yet fully exploited in the field of dispersions, emulsions especially for highly complex food relevant systems. In general, SANS and SAXS are useful tools to capture form and structure factors of samples ranging from biomolecules, polymers, liquid crystals, emulsions and colloidal suspensions in a range from nm to μm length scale [45]. Thus, SANS and SAXS are valuable to compare the form and structure of biomolecules like proteins in water solutions and in emulsions including protein shape and size, interfacial layer thickness, and oil droplet size in emulsions as performed for fish oil-in-water emulsions and caseinate stabilized oil-in-water emulsions [35,36].

However, these publications do not cover the full potential of the methods SANS and SAXS. Contrast variation is a powerful tool for SANS measurements. Adjustment of the deuterium and hydrogen portion in the water, oil phase or interface highlights the different phases or the interface in emulsions. Thus, within a series of measurements, contrast variation delivers the whole picture of the emulsion, but the interface, the water and oil phase are analyzed separately from each other. The previously mentioned publications did not perform a contrast variation of the oil phase in the most accurate way, which is a comparison of a deuterated and hydrogenated triacylglyceride-oil [35,36]. The use of deuterated hexadecane or toluene in comparison to a triacylglyceride-oil strongly impacts the interfacial properties of protein and phospholipids due

to significantly changed interactions between the hydrophobic phase and protein or phospholipid as indicated in [24–26,46,47]. Further, an analytical or literature-based consideration of the CIC of the used protein was not included [35,36], as well as a comparison of the protein molecule structure in water solution and in emulsions via a coarse-grained based modelling [35,36] like DENFERT [48].

Therefore, we aim to broaden and improve the interfacial and emulsion characterization methods, since we focus on details of macro- and microscale of emulsions at the same time within the same emulsion. Thus, we identify the oil droplet size, but also details of the interfacial layer including interface coverage and especially molecular rearrangement within one experiment. In detail, we show an approach to expand the understanding for various emulsions using SANS and SAXS: via usage of accurate contrast variation of deuterated and hydrogenated water and triacylglyceride-oil phase for SANS measurements, and followed via improved data analysis including coarse grained modelling.

As a starting point, we consider the protein concentration covering a concentration range around the proteins CIC. We hypothesize that we are able to determine the CIC via SAXS analysis as long as a change in protein molecule structure, thus a change in protein shape, takes place during the protein migration, adsorption and unfolding steps.

Therefore, we compare the protein solubilized in water with protein stabilized emulsions at the same protein concentration, as a function of concentration. For the emulsion, the change in protein shape will be detectable for any concentration below the CIC, since above the CIC the protein is also located in the water phase. For β-lactoglobulin at pH 7, we expect a change from the dimeric and globular protein organization in the water phase, to a more unfolded protein shape at the oil/water interface at a protein concentration at or below the CIC with up to 0.25% for β-lactoglobulin.

Further, we hypothesize that we are able to determine the change in protein molecule structure, thus a change in protein shape taking place during the protein migration, adsorption and unfolding steps also above the CIC via SANS and contrast variation, applying also coarse-grained modelling.

Therefore, we compare β-lactoglobulin solubilized in $D_2O$ and β-lactoglobulin stabilized emulsions at pH 7 at the CIC with 0.25% protein and above the CIC with 0.50% protein with different contrasts. The oil/water interface is highlighted with the use of deuterated triacylglyceride-oil and $D_2O$ (*interfacial protein contrast*). The oil droplets with the oil/water interface are highlighted with the use of hydrogenated triacylglyceride-oil and $D_2O$. The oil droplets without the

oil/water interface are highlighted with the use of deuterated triacylglyceride-oil, and 60/40 ratio of $H_2O$ and $D_2O$ to match the protein scattering length density (*protein contrast match*). A fully hydrogenated emulsion is investigated as well. By doing so, the water, oil phase and interface are highlighted separately from each other, resulting in a complete picture of the emulsion.

The concentration series via SAXS, and the contrast variation via SANS improve the understanding of β-lactoglobulin stabilized emulsions. This approach may be extended to a series of proteins with different molecular size, structure under usage of different external parameters like pH and ionic strength, to expand the understanding for various emulsions using SANS and SAXS.

## 2. Materials and Methods

### 2.1 Materials

The raw materials were either purchased or synthesized. β-lactoglobulin (β-lg) was purchased from *Sigma Aldrich Chemie GmbH* (Steinheim, Germany) with a purity of 99.5%. Hydrogenated medium-chain-triacylglyceride-oil (*h*-MCT-oil) WITARIX® MCT 60/40 was kindly provided from *IOI Oleo GmbH* (Hamburg, Germany). Interfacial active substances in the MCT-oil were removed via magnesium silicate adsorption (Florisil®, *Carl Roth GmbH,* Karlsruhe Germany). Deuterated medium-chain-triacylglyceride-oil (*d*-MCT-oil) with a purity of ≥99% and a deuteration degree of ≥91% was synthesized using deuterated glycerol as well as deuterated caprylic and capric acid. The fatty acids were used in a 60/40 ratio of caprylic and capric acid to match the utilized *h*-MCT-oil. For *d*-MCT-oil, glycerol-$d_8$ (99% D) was purchased from *Eurisotop SAS, Cambridge Isotope Laboratories Inc.*. The deuterated fatty acids were kindly provided by the ISIS deuteration facility. A specialized and byproduct free synthesis method for triacylglyceride-oils was developed. Details about the synthesis are published [49]
For protein solutions, and emulsions, 0.05 to 0.75% β-lg were solubilized in $D_2O$, distilled $H_2O$ or 40/60 $D_2O$/ $H_2O$ under stirring conditions, the pD/pH was adjusted with <1 µL 0.1M D/HCL, and the solution were stored for at least 12 h at 4 °C. 5% *d*/*h*-MCT-oil were dispersed in 0.05 to 0.75% β-lg solutions. The emulsification was performed at 25 000 rpm for 4 min with a small probe in a T18 digital Ultraturrax from *IKA® GmbH and Co.KG* (Breisgau, Germany). The oil droplet size distribution of all hydrogenated emulsions was measured with a laser scattering

particle size distribution analyzer LA-960V2 from *Horiba, Ltd.* (Kyoto, Japan) using a refractive index of n=1.45 for the oil phase, and n=1.33 for the water phase. The measurements were performed at least in triplicate. Three percentiles of the oil droplet size distribution - D10, D50 and D90 - of all emulsions varied between 2.09 ± 0.12 μm, 3.52 ± 0.27 μm and 6.36 ± 0.82 μm, respectively.

## 2.2 SAXS

SAXS experiments were performed using a laboratory based SAXS/WAXS/USAXS beamline KWS-X (XENOCS XEUSS 3.0 XL Garching Version) at JCNS MLZ. The X-ray source is a D2+ MetalJet (Excillum) with a liquid metal anode operating at 70 kV and 3.57 mA with Ga-Kα radiation (wavelength $\lambda$ = 1.314 Å). Samples were measured in a glass capillary (1.5 mm ID) that was kept at room temperature. The sample to detector distances were set from 0.50 m to 1.70 m, which cover the scattering vector Q range from 0.005 to 1.100 $Å^{-1}$ (Q is the scattering vector, $Q=(4\pi/\lambda)\sin(\theta)$, $2\theta$ is the scattering angle). The scattering patterns were obtained with 600 s exposure time, were repeated for 6 to 12 times, and were measured at least in triplicate for each protein concentration either in solution or in emulsion. The SAXS patterns were normalized to an absolute scale and azimuthally averaged to obtain the intensity profiles, and the solvent background was subtracted. Data were fitted with sasview 5.0.4 using the dimeric cylindrical and core shell elliptical bicelle model. For the dimeric cylindrical model [50], two cylinders on the same axis are separated by a thin layer of 0.2 nm, and an electron density changed by the same factor as the electron density between solvent and cylinders. The core shell elliptical bicelle model [51] was used with the following geometrical constraints: the core was set to the same electron density as the solvent, the core was surrounded by a rim of 0.5 nm thickness and faces of the elliptical cylindrical core also with 0.5 nm thickness. The electron density was changed by a factor of 1/6 for the rim and ½ for the faces of the bicelle. Since the scaling of the fits have been used as a free parameter, the electron density contrast can be only regarded as a relative contrast change. The large axis of the ellipsoidal particle was stretched by two compared to the small axis. The model is certainly a simplification of the actual β-lg protein, whose electron density is e.g., shown in [52]. Also, hydration shell water might contribute to a variation of the electron density at the outer surface of the protein, as reported in [53]. But in the context of showing possible coarse-grained structural changes between bulk and interface β-lg the model used here is the simplest option to describe the changes of the first minima in the experimental data by a change of the overall structure. More details of the fitting models are presented in the SI.

### 2.3. SANS

SANS experiments were carried out at the SANS-I at the Swiss Spallation Neutron Source (SINQ), Paul Scherrer Institute, Switzerland using a wavelength $\lambda$ = 5 Å and a wavelength resolution $\Delta\lambda/\lambda$ = 10% [54]. The samples were filled in quartz cuvettes with 2 and 4 mm path length during SANS measurements. Cuvettes were aligned using the thermostatic sample holder at a fixed temperature of 25°C. A two-dimensional (96×96 $cm^2$) $^3He$ gas detector was used for the detection of scattered neutrons. Two sample-to-detector distances of 2 m and 8 m were used to cover the wave vector transfer Q-range from 0.0075 to 0.65 $Å^{-1}$. The raw data were radially averaged, corrected for electronic background and empty cell background using the BerSANS software [55]. A sample with $H_2O$ has been measured, which illuminates the detector homogeneously due to the strong isotropic incoherent scattering of water and is required for the detector calibration. All data were normalized by the $H_2O$ scattering to obtain absolute scale. Technical details can be found here [56].

For the data analysis, we calculated the scattering length densities (SLD) of all components using the NIST SLD calculator. The values are tabulated in **Table1**. We refer to hydrogenated and deuterated components, while for β-lg we assume a natural exchange with the water phase. Data analysis was performed via DENFERT modeling, and further derived calculations.

## 3. Results and Discussion

### 3.1. SAXS

Comparative concentration series of β-lg solubilized in distilled water and β-lg stabilized emulsions at pH 7 were performed via SAXS (**Fig.1**). For all samples, a *Guinier scattering* of β-lg is identified at 0.03 $Å^{-1} < Q < 0.10$ $Å^{-1}$ followed by fringes from the internal protein scattering at $Q > 0.20$ $Å^{-1}$(in the SI, the SAXS data are also shown in the Guinier representation). For β-lg solubilized in distilled water (**Fig.1a**), two maxima at $Q = 0.29$ $Å^{-1}$ and 0.53 $Å^{-1}$ are identified. The intensity of the maxima is reduced with decreasing protein concentration. For β-lg stabilized emulsions (**Fig.1b**), two maxima at $Q = 0.29$ $Å^{-1}$ and 0.53 $Å^{-1}$ are identified, if the protein concentration is above 0.25%. Below and at a protein concentration of 0.25%, a single maximum at $Q = 0.33$ $Å^{-1}$ is shown, which indicates a change in the protein shape, thus protein structure due to adsorption at the oil/water interface with followed partial protein unfolding. This shift in structural information is indicated by the dashed lines in **Fig.1**.

In detail, β-lg solubilized in distilled water at pH 7 is organized as a dimer [10–12] which is indicated by all shown structural features in the SAXS curves in **Fig.1a**. With decreasing concentrations, the maxima are less pronounced due to the low amount of scattering material. β-lg stabilized emulsions at pH 7 with a protein concentration higher than 0.25% show a similar scattering pattern like the water solubilized β-lg **Fig.1b**. The β-lg in these emulsions is located at the interface and in the water phase due to a protein concentration above the CIC. The CIC was earlier identified at 0.10% mostly up to 0.25% [8,32]. β-lg stabilized emulsions at pH 7 with a protein concentration of 0.25% or lower show only the partly unfolded protein located at the interface as earlier indicated by [8].

These assumptions were approved with data fitting of the SAXS curves using the core shell elliptical bicelle or the dimeric cylindrical model (**Table2**) using SasView5 (www.sasview.org) and the corresponding built-in models. More details are given in the SI. The dimeric cylindrical model [50] applies to all β-lg solutions and to β-lg stabilized emulsions above a protein concentration of 0.25%. This model identified two domains thus dimeric β-lg molecules with an overall length of 6 nm and a diameter of 3.5 nm. The two cylinders were separated by a very short gap (0.1 nm in the fits). The core shell elliptical bicelle model [51] applies to β-lg stabilized emulsions at or below a protein concentration of 0.25%, which approves the change in the protein shape and protein structure due to interfacial adsorption. At the interface, the protein has, according to the present model, a shape with 8 nm diameter and a height of 2 nm, i.e. an oblate and slightly more extended geometry. It was fitted with a hollow interior and 0.5 nm layers at the rim and the surfaces of the cylinder model. Since the actual rearrangement of the β-lg at the interface is more complicated than a centrosymmetric shape change, these models will not represent the full details of molecular changes where hydrophobic groups expose more towards the oil phase. But they show that with the argument of a slight overall shape change the shift of the minima can be explained. More details might be accessible if the actual molecular structure at the interface can be simulated on sufficiently long-time scales with molecular dynamics simulations.

### 3.2. SANS

β-lg stabilized emulsions at pH 7 were compared using the CIC of β-lg with 0.25% and a concentration above the CIC with 0.50%, via SANS measurements with different contrasts as displayed in **Fig.2.**

In general, we believe that the SANS data is more accurate than the SAXS data in terms of the more homogenous SLD, thus high neutron contrast within the β-lg molecule. The protein scattering is observable in all contrasts (except for the *protein contrast match,* i.e. $H_2O/D_2O$ (60/40 ratio) and *d*-MCT-oil) in the Q-range from 0.07 to 0.30 $Å^{-1}$. At higher Q, the scattering patterns fade out in the statistical noise. This is due to randomness and disorder on a rather small scale. The randomness and disorder seem to be connected to not separately packed proteins in the water phase, and at the interface. First, the β-lg molecule at pH 7 is located as dimer in the water phase [12]. Secondly, the β-lg molecule partly unfolds at the interface [8,15,16,18]. Both phenomena cause a certain degree of randomness and disorder. Details about this issue remain to be discussed. The very high-*Q* end displays an upturn from the incoherent background that is emphasized by the subtraction of a constant background and is caused by a variation of the optical path length towards higher *Q* [57]. At lower Q, a classical *Porod scattering* from the oil droplets for two contrasts ($D_2O$ and *h*-MCT-oil; $H_2O/D_2O$ (60/40 ratio) and *d*-MCT-oil) is visible. Only the very lowest $Q < 0.013$ $Å^{-1}$ display an upturn that we discuss below. The interfacial protein contrast ($D_2O$ and *d*-MCT-oil) displays interface scattering ($\sim Q^{-2}$) at low Q from the interface coverage of the protein on the oil. The curves of the *interfacial protein contrast* are comparable for both protein concentrations above (0.50%) and at the CIC (0.25%). The fully hydrogenated sample reflects a very noisy protein scattering. For the current manuscript we omit the analysis of this curve.

In detail, the *Porod* and *interface scattering* were used as calculation basis for the average oil droplet size radius, the protein concentration at the interface and in solution, and the interfacial thickness. The calculation was derived as followed:

For analyzing the scaling behavior of the scattering pattern at low Q, we employed the classical *Porod scattering formula* [58] and a formula for the *interface scattering*. We summarize the results here:

$$I_{\text{Porod}} = 2\pi(\Delta\rho_{\text{oil}})^2\phi_{\text{oil}}\frac{S_{\text{oil}}}{V_{\text{oil}}}C_{\text{Porod}}Q^{-4} \quad (1)$$

$$I_{\text{Interface}} = 2\pi(\Delta\rho_P)^2\phi_{\text{Ps}}\phi_{\text{oil}}\frac{3d_{\text{Ps}}^2}{R_{\text{oil}}}C_{\text{interface}}Q^{-2} \quad (2)$$

These simple power laws reflect the relatively large polydispersity of the droplet radius $R_{oil}$ in the sense that heavy oscillations of the form factors smear sufficiently out such that the only remaining Q-dependence of the form factors is exactly that power law (see also SI). The well-known *Porod formula* introduces the volume fraction of the droplet (oil) phase $\phi$ and the interface to volume ratio $S_{oil}/V_{oil} = 3/R_{oil}$ for spheres with a radius $R_{oil}$ in 3 dimensions. This *Porod scattering* is observed for hydrogenated oil in heavy water (and hydrogenated protein). We derived a similar formula for the sphere interface scattering (eq. 2, see SI) and obtained the classical $Q^{-2}$ power law. However, the observed scattering refers to a *protein contrast* (hydrogenated protein in $D_2O$ and deuterated oil). So, the amount of scattering material is reflected by the magnitude $d_{Ps}$, the effective protein layer thickness, and $\phi_{Ps}$, the protein volume fraction at the oil interface.

When evaluating the droplet radius from the *Porod scattering* (eq. 1) without polydispersity ($C_{Porod} = 1$) the resulting radius is approx. $R_{oil} = 0.64 \pm 0.03$ µm for both protein concentrations stabilizing the emulsions. Taking the full polydispersity correction (see SI) into account we arrive at $R_{oil} = 1.69 \pm 0.09$ µm, which matches well the value of approx. $1.76 \pm 0.14$ µm obtained from the static light scattering particle sizer. For polydispersity corrections ($C_{Porod}$ and $C_{interface}$) we also refer to the literature [59].

For further interpretation of the effective thickness $d_{Ps}$, we compared the volume and interface scattering (eqs. 1 and 2) and form the ratio:

$$\frac{I_{interface}}{I_{Porod}} Q^{-2} = \left(\frac{\Delta\rho_P}{\Delta\rho_{oil}}\right)^2 \phi_{Ps} d_{Ps}^2 \frac{C_{interface}}{C_{Porod}}$$

For this calculation, we fitted the power laws independently in their respective $Q$-range (there is little or no overlap, see **Fig.2** straight lines. Porod: $0.017Å^{-1} < Q < 0.03Å^{-1}$ and surface scattering: $0.007Å^{-1} < Q < 0.019Å^{-1}$). The calculated interfacial coverage is $\phi_{Ps} = 91\%$ and 79% for the two protein concentrations of 0.25% and 0.50% stabilizing the emulsions respectively (we used a protein layer thickness of $d_{Ps} = 27Å$ [12]). The two different interfacial coverages give an impression about the precision of this measurement, because we believe they should be identical. The calculation is independent on the exact shape of the oil droplet interface, because we

refer to relative amplitudes of the *Porod and interface scattering* (eqs. 1 and 2) and use the interface to volume ratio obtained from the two power laws.

The low-Q upturn (**Fig.2**) is of a still unclear origin and may point towards an intermediate scale structure between oil droplets and proteins. One possibility could be the not 100% compact packing of the proteins at the oil interface. In the future, we would like to address this topic using VSANS that could be performed on KWS-3, Maier-Leibnitz-Zentrum (FRM II, Forschungsreaktor München II) in Garching [60].

Further, the corrected data sets of β-lg in solution and β-lg stabilized emulsions with 0.25% and 0.50% protein concentrations were analyzed via DENFERT software [48] focusing on a pair distribution function $p(r)$ and a reconstructed real space structure (**Fig.3**). For the protein contrast, we fitted a structure factor with an elliptical form factor at $Q < 0.2 Å^{-1}$ in order to remove the structure factor by division. The then used data between $Q = 0.015 Å^{-1}$ and $0.27 Å^{-1}$ reflects the intensity decay from the Guinier range to the first minimum, i.e., possible fringes are completely neglected. This approach agrees with the DENFERT software that delivers both: $p(r)$ and a real space reconstruction, i.e., the internal structure is neglected. The pair distribution function turns to zero at the maximum extension of the globular particle. The real space reconstruction displays one representative constitution to which errors usually are not given. Multiple runs of the software would result in multiple reconstructions. While at 0.25%, we expect that almost all protein is covering the oil interface [8], at 0.50% at least 50% of the protein is covering the interface. At the lower concentration, we see an extension of the protein of approx. 57 Å being larger than $2R_p = 42.4$ Å and an unfolding of the protein in two leaflets in the real space reconstruction. According to FTIR and CD analysis, β-lg loses secondary structure features as soon as adsorbed at the oil/water interface leading to a more random coil structure, and intermolecular β-sheets [8,15–18]. So, we can conclude that the protein is more likely found as associated protein molecules at the oil interface in a slightly unfolded state. The scattering reflects a superposition of associated monomer at the interface and dimers [52,61] in the bulk. The unfolding of the protein becomes quite clear by comparing the real space structures obtained from DENFERT (**Fig.3**). For the emulsion state, a clear cleft is visible, while the solution structure looks smoother indicating the dimer structure of two compact globuli. The extension here also stays at around 55 Å. The cleft reflects the unfolding of the dimer with the hydrophobic surface towards the oil droplet.

All results indicate for 0.25% and 0.50% protein in emulsions, a comparable protein unfolding after protein adsorption at the interface. No multilayer formation of β-lg at the interface was

detected or calculated. This understanding is rather new, and contrasts results presented in [8,13].

The success of the DENFERT algorithm for SANS data is due to the constant high neutron contrast when looking along the protein chain for the different amino acids against $D_2O$. So, for neutrons the protein really looks globular, and higher-*Q* fringes are widely suppressed. This is completely different for the SAXS data. For SAXS, the contrast against water becomes virtually zero for some parts of the protein, and so the protein looks discontinuous. This is based on the electrical double layer of counterions [62] around the negatively charged β-lg molecule at pH 7 [31]. These counterions are most likely chloride ions from the pH adjustment and natural available ions like sodium or manganese, which are affecting the scattering length density of the protein molecule strongly. However, due to the contrast against water the SAXS data shows the beautiful higher-*Q* fringes (**Fig.1**) that allow to distinguish the different states at the oil interface vs. the dispersion state. Contrarily, the modeling of the fringes becomes tedious and was not covered completely by our modeling via DENFERT.

We therefore note that a combination of SAXS and SANS provides detailed and valuable information on the conformation of β-lg at the oil-water-interface. Using SAXS, we find that β-lg is in the dimer state in dilute solution. In the emulsion, we clearly find a shape transition at the CIC, where for c > CIC, we observe the dimer state, whereas for c < CIC we observe an unfolded state. With SANS for $D_2O$/*d*-MCT-contrast, we clearly observe the $Q^{-4}$ *Porod scattering* at low-*Q*, from which we can derive the radius of the emulsion droplets, and the *protein scattering* at high-*Q*, which can be used to determine the protein conformation. With SANS in $D_2O$/*d*-MCT-contrast, we clearly observe the $Q^{-2}$ scattering of the interface, from which we can estimate the interfacial coverage, as well as the *protein scattering* at high-*Q*. When the protein is matched in $H_2O$/$D_2O$/*d*-MCT-contrast, we only observe the $Q^{-4}$ Porod scattering of the emulsion droplets, without any contribution of protein scattering, demonstrating the great potential of contrast variation for structure determination of emulsion systems.

## 4. Conclusions

Neutron- and X-ray scattering are valuable methods to improve our current understanding of protein-stabilized emulsions. Especially neutron scattering offers additional and simultaneous information of the interfacial layer in emulsions in comparison to established methods like FTIR [8]. Contrast variation within neutron scattering assists to focus either on the interface,

the oil or water phase, resulting in information of either the oil droplet size, interfacial layer thickness, protein concentration at the interface, and protein shape at the interface.

In comparison to current scattering literature [35,36], new approaches with consideration of a relevant triacylglyceride-oil and of the proteins CIC, with accurate contrast variation, and improved data analysis including coarse grained modelling were presented. These new approaches improved and specified the output of X-ray- and neutron scattering data with focus on the protein interfacial layer, which is applicable for various emulsions.

As a starting point, this study focused on the protein concentration dependent effects. At and below the proteins CIC, the change in the protein shape thus protein structure during interfacial adsorption with followed protein unfolding could be detected via SAXS analysis. Below and above the CIC of the protein, SANS with contrast variation and coarse-grained modelling identified also the change in protein shape at the interface. For a protein concentration at and above the CIC, the interfacial layer thickness and the protein interfacial coverage via $Q^{-2}$ scattering of the interface could be determined, as well as the protein shape via *protein scattering* at high-*Q* for β-lg at pH 7. We could state that the interfacial coverage at and above the CIC is almost complete, i.e., $\phi_{Ps}$ = 91% and 79% using the intensity ratio of the oil and protein contrast in SANS measurements. No indication for multilayer formation via increased interfacial layer thickness could be identified, as stated in previous literature [13]. Since SANS with accurate contrast variation highlights the interface in comparison to other techniques like FTIR [8], the presented results show a high impact to understand protein-stabilized interfaces in emulsions. This approach may be extended to a series of proteins with different molecular size, structure under usage of different external parameters like pH and ionic strength, and via implementation of MD simulations. By doing so, our understanding of interfaces will be strongly improved to enhance the stabilization and to tailor the properties of protein-stabilized oil-in-water emulsions.

**Acknowledgements**

The authors gratefully acknowledge the help during synthesis of MCT-oil: via synthesis of fatty acids by the ISIS deuteration facility with special help from Yao Chen and Peixun Li, and via theoretical and methodical input from Jürgen Allgaier located at the Deuteration lab of the Forschungszentrum Jülich GmbH. Further, Alexandros Koutsioumpas helped with discussions to coarse grained modelling of protein structure/shape.

## References


[1] D.J. McClements, C.E. Gumus, Natural emulsifiers — Biosurfactants, phospholipids, biopolymers, and colloidal particles: Molecular and physicochemical basis of functional performance, Adv Colloid Interface Sci. 234 (2016) 3–26. https://doi.org/10.1016/j.cis.2016.03.002.

[2] D.J. McClements, S. Mahdi Jafari, Improving emulsion formation, stability and performance using mixed emulsifiers: A review, Adv Colloid Interface Sci. 251 (2018) 55–79. https://doi.org/10.1016/j.cis.2017.12.001.

[3] D. Guzey, D.J. McClements, Formation, stability and properties of multilayer emulsions for application in the food industry, Adv Colloid Interface Sci. 128–130 (2007) 227–248. https://doi.org/10.1016/j.cis.2006.11.021.

[4] F. Ravera, K. Dziza, E. Santini, L. Cristofolini, L. Liggieri, Emulsification and emulsion stability: The role of the interfacial properties, Adv Colloid Interface Sci. 288 (2021) 102344. https://doi.org/10.1016/j.cis.2020.102344.

[5] E. Dickinson, Mixed biopolymers at interfaces: Competitive adsorption and multilayer structures, Food Hydrocoll. 25 (2011) 1966–1983. https://doi.org/10.1016/j.foodhyd.2010.12.001.

[6] E. Dickinson, An introduction to food colloids, Oxford University Press, Oxford, United Kingdom, 1992.

[7] R.S.H. Lam, M.T. Nickerson, Food proteins: A review on their emulsifying properties using a structure-function approach, Food Chem. 141 (2013) 975–984. https://doi.org/10.1016/j.foodchem.2013.04.038.

[8] H. Schestkowa, S. Drusch, A.M. Wagemans, FTIR analysis of β-lactoglobulin at the oil/water-interface, Food Chem. 302 (2020) 125349. https://doi.org/10.1016/j.foodchem.2019.125349.

[9] B. Zhou, J.T. Tobin, S. Drusch, S.A. Hogan, Interfacial properties of milk proteins: a review, Adv Colloid Interface Sci. 295 (2021) 102347. https://doi.org/10.1016/j.cis.2020.102347.

[10] D. Mercadante, L.D. Melton, G.E. Norris, T.S. Loo, M.A.K. Williams, R.C.J. Dobson, G.B. Jameson, Bovine β-lactoglobulin is dimeric under imitative physiological conditions: Dissociation equilibrium and rate constants over the pH range of 2.5-7.5, Biophys J. 103 (2012) 303–312. https://doi.org/10.1016/j.bpj.2012.05.041.

[11] G. Baldini, S. Beretta, G. Chirico, H. Franz, E. Maccioni, P. Mariani, F. Spinozzi, Salt-induced association of β-lactoglobulin by light and X-ray scattering, Macromolecules. 32 (1999) 6128–6138. https://doi.org/10.1021/ma990709u.

[12] L. Anghel, A. Rogachev, A. Kuklin, R.V. Erhan, β-Lactoglobulin associative interactions: a small-angle scattering study, European Biophysics Journal. 48 (2019) 285–295. https://doi.org/10.1007/s00249-019-01360-9.

[13] J. Krägel, S.R. Derkatch, R. Miller, Interfacial shear rheology of protein-surfactant layers, Adv Colloid Interface Sci. 144 (2008) 38–53. https://doi.org/10.1016/j.cis.2008.08.010.

[14] R. Miller, J.K. Ferri, A. Javadi, J. Krägel, N. Mucic, R. Wüstneck, Rheology of interfacial layers, Colloid Polym Sci. 288 (2010) 937–950. https://doi.org/10.1007/s00396-010-2227-5.

[15] L. Day, J. Zhai, M. Xu, N.C. Jones, S. V. Hoffmann, T.J. Wooster, Conformational changes of globular proteins adsorbed at oil-in-water emulsion interfaces examined by synchrotron radiation circular dichroism, Food Hydrocoll. 34 (2014) 78–87. https://doi.org/10.1016/j.foodhyd.2012.12.015.

[16] J. Zhai, T.J. Wooster, S. V. Hoffmann, T.H. Lee, M.A. Augustin, M.I. Aguilar, Structural rearrangement of β-lactoglobulin at different oil-water interfaces and its

effect on emulsion stability, Langmuir. 27 (2011) 9227–9236. https://doi.org/10.1021/la201483y.
[17] J. Zhai, A.J. Miles, L.K. Pattenden, T.-H. Lee, M.A. Augustin, B.A. Wallace, M.-I. Aguilar, T.J. Wooster, Changes in beta-lactoglobulin conformation at the oil/water interface of emulsions studied by synchrotron radiation circular dichroism spectroscopy., Biomacromolecules. 11 (2010) 2136–2142. https://doi.org/10.1021/bm100510j.
[18] Y. Fang, D.G. Dalgleish, Conformation of β-Lactoglobulin studied by FTIR: Effect of pH, temperature, and adsorption to the oil–water interface, J Colloid Interface Sci. 196 (1997) 292–298. https://doi.org/10.1006/jcis.1997.5191.
[19] Y. Dickinson, E. and Matsumura, Time dependent polymerisation of beta lactoglobulin through disulphide bonds at the oil water interface in emulsions, Int. J. Biol. Macromol. 13 (1991) 27–30.
[20] D.A. Kim, M. Cornec, G. Narsimhan, Effect of thermal treatment on interfacial properties of β-lactoglobulin, J Colloid Interface Sci. 285 (2005) 100–109. https://doi.org/10.1016/j.jcis.2004.10.044.
[21] H. Kieserling, P. Giefer, M.J. Uttinger, V. Lautenbach, T. Nguyen, R. Sevenich, C. Lübbert, C. Rauh, W. Peukert, U. Fritsching, S. Drusch, A. Maria Wagemans, Structure and adsorption behavior of high hydrostatic pressure-treated β-lactoglobulin, J Colloid Interface Sci. 596 (2021) 173–183. https://doi.org/10.1016/j.jcis.2021.03.051.
[22] J.K. Keppler, A. Heyse, E. Scheidler, M.J. Uttinger, L. Fitzner, U. Jandt, T.R. Heyn, V. Lautenbach, J.I. Loch, J. Lohr, H. Kieserling, G. Günther, E. Kempf, J.H. Grosch, K. Lewiński, D. Jahn, C. Lübbert, W. Peukert, U. Kulozik, S. Drusch, R. Krull, K. Schwarz, R. Biedendieck, Towards recombinantly produced milk proteins: Physicochemical and emulsifying properties of engineered whey protein beta-lactoglobulin variants, Food Hydrocoll. 110 (2021) 106132. https://doi.org/10.1016/j.foodhyd.2020.106132.
[23] R. Wüstneck, B. Moser, G. Muschiolik, Interfacial dilational behaviour of adsorbed β-lactoglobulin layers at the different fluid interfaces, Colloids Surf B Biointerfaces. 15 (1999) 263–273. https://doi.org/10.1016/S0927-7765(99)00093-4.
[24] J. Bergfreund, P. Bertsch, P. Fischer, Adsorption of proteins to fluid interfaces: Role of the hydrophobic subphase, J Colloid Interface Sci. 584 (2021) 411–417. https://doi.org/10.1016/j.jcis.2020.09.118.
[25] J. Bergfreund, P. Bertsch, P. Fischer, Effect of the hydrophobic phase on interfacial phenomena of surfactants, proteins, and particles at fluid interfaces, Curr Opin Colloid Interface Sci. 56 (2021) 101509. https://doi.org/10.1016/j.cocis.2021.101509.
[26] J. Bergfreund, P. Bertsch, S. Kuster, P. Fischer, Effect of oil hydrophobicity on the adsorption and rheology of β-Lactoglobulin at oil-water interfaces, Langmuir. 34 (2018) 4929–4936. https://doi.org/10.1021/acs.langmuir.8b00458.
[27] S.R. Euston, R.L. Hirst, J.P. Hill, The emulsifying properties of β-lactoglobulin genetic variants A, B and C, Colloids Surf B Biointerfaces. 12 (1999) 193–202. https://doi.org/10.1016/S0927-7765(98)00074-5.
[28] A. Moro, G.D. Báez, P.A. Busti, G.A. Ballerini, N.J. Delorenzi, Effects of heat-treated b -lactoglobulin and its aggregates on foaming properties, Food Hydrocoll. 25 (2011) 1009–1015. https://doi.org/10.1016/j.foodhyd.2010.09.021.
[29] P.A. Rühs, C. Affolter, E.J. Windhab, P. Fischer, Shear and dilatational linear and nonlinear subphase controlled interfacial rheology of β-lactoglobulin fibrils and their derivatives, J Rheol (N Y N Y). 57 (2013) 1003–1022. https://doi.org/10.1122/1.4802051.
[30] P.A. Rühs, N. Scheuble, E.J. Windhab, R. Mezzenga, P. Fischer, Simultaneous control of ph and ionic strength during interfacial rheology of β-lactoglobulin fibrils adsorbed

at liquid/liquid interfaces, Langmuir. 28 (2012) 12536–12543. https://doi.org/10.1021/la3026705.
[31] H. Schestkowa, T. Wollborn, A. Westphal, A.M. Wagemans, U. Fritsching, S. Drusch, Conformational state and charge determine the interfacial stabilization process of beta-lactoglobulin at preoccupied interfaces, J Colloid Interface Sci. 536 (2019) 300–309. https://doi.org/10.1016/j.jcis.2018.10.043.
[32] F. Tamm, Impact of an Enzymatic Hydrolysis on the Functional Properties of Globular Proteins, 2016.
[33] A. Moro, G.D. Báez, G.A. Ballerini, P.A. Busti, N.J. Delorenzi, Emulsifying and foaming properties of β -lactoglobulin modi fi ed by heat treatment, FRIN. 51 (2013) 1–7. https://doi.org/10.1016/j.foodres.2012.11.011.
[34] Y.T. Hu, Y. Ting, J.Y. Hu, S.C. Hsieh, Techniques and methods to study functional characteristics of emulsion systems, J Food Drug Anal. 25 (2017) 16–26. https://doi.org/10.1016/j.jfda.2016.10.021.
[35] B. Yesiltas, M. Torkkeli, L. Almásy, Z. Dudás, A.F. Wacha, R. Dalgliesh, P.J. García-Moreno, A.D.M. Sørensen, C. Jacobsen, M. Knaapila, Interfacial structure of 70% fish oil-in-water emulsions stabilized with combinations of sodium caseinate and phosphatidylcholine, J Colloid Interface Sci. 554 (2019) 183–190. https://doi.org/10.1016/j.jcis.2019.06.103.
[36] L. Cheng, A. Ye, Z. Yang, E.P. Gilbert, R. Knott, L. de Campo, B. Storer, Y. Hemar, H. Singh, Small-angle X-ray scattering (SAXS) and small-angle neutron scattering (SANS) study on the structure of sodium caseinate in dispersions and at the oil-water interface: Effect of calcium ions, Food Structure. 32 (2022) 100276. https://doi.org/10.1016/j.foostr.2022.100276.
[37] M.L. Johns, NMR studies of emulsions, Curr Opin Colloid Interface Sci. 14 (2009) 178–183. https://doi.org/10.1016/j.cocis.2008.10.005.
[38] R. Bernewitz, G. Guthausen, H.P. Schuchmann, NMR on emulsions: characterisation of liquid dispersed systems, Magnetic Resonance in Chemistry. 49 (2011) S93–S104. https://doi.org/10.1002/mrc.2825.
[39] T. Heiden-Hecht, M. Ulbrich, S. Drusch, M. Brückner-Gühmann, Interfacial properties of β-lactoglobulin at the oil/water interface: influence of starch conversion products with varying dextrose equivalents, Food Biophys. 16 (2021) 169–180. https://doi.org/10.1007/s11483-020-09658-4.
[40] L.M.C. Sagis, P. Fischer, Nonlinear rheology of complex fluid-fluid interfaces, Curr Opin Colloid Interface Sci. 19 (2014) 520–529. https://doi.org/10.1016/j.cocis.2014.09.003.
[41] X. Zhou, G. Sala, L.M.C. Sagis, Bulk and interfacial properties of milk fat emulsions stabilized by whey protein isolate and whey protein aggregates, Food Hydrocoll. 109 (2020) 106100. https://doi.org/10.1016/j.foodhyd.2020.106100.
[42] D. Zare, K.M. McGrath, J.R. Allison, Deciphering β-lactoglobulin interactions at an oil-water interface: A molecular dynamics study, Biomacromolecules. 16 (2015) 1855–1861. https://doi.org/10.1021/acs.biomac.5b00467.
[43] L.C. Ter Beek, M. Ketelaars, D.C. McCain, P.E.A. Smulders, P. Walstra, M.A. Hemminga, Nuclear magnetic resonance study of the conformation and dynamics of β-casein at the oil/water interface in emulsions, Biophys J. 70 (1996) 2396–2402. https://doi.org/10.1016/S0006-3495(96)79807-7.
[44] H. Arwin, Spectroscopic ellipsometry and biology: recent developments and challenges, Thin Solid Films. 313 (1998) 764–774. https://doi.org/10.1016/s0040-6090(97)00993-0.

[45] C.M. Jeffries, J. Ilavsky, A. Martel, S. Hinrichs, A. Meyer, J.S. Pedersen, A. V. Sokolova, D.I. Svergun, Small-angle X-ray and neutron scattering, Nature Reviews Methods Primers. 1 (2021) 1–70. https://doi.org/10.1038/s43586-021-00064-9.
[46] T. Heiden-Hecht, S. Drusch, Impact of saturation of fatty acids of phosphatidylcholine and oil phase on properties of β-lactoglobulin at the oil/water interface, Food Biophys. 17 (2021) 171–180. https://doi.org/10.1007/s11483-021-09705-8.
[47] E. Hildebrandt, A. Dessy, J.H. Sommerling, G. Guthausen, H. Nirschl, G. Leneweit, Interactions between phospholipids and organic phases: Insights into lipoproteins and nanoemulsions, Langmuir. 32 (2016) 5821–5829. https://doi.org/10.1021/acs.langmuir.6b00978.
[48] A. Koutsioubas, S. Jaksch, J. Pérez, DENFERT version 2: Extension of ab initio structural modelling of hydrated biomolecules to the case of small-angle neutron scattering data, J Appl Crystallogr. 49 (2016) 690–695. https://doi.org/10.1107/S1600576716003393.
[49] K. Schwärzer, T. Heiden-Hecht, Y. Chen, O. Holderer, H. Frielinghaus, P. Li, J. Allgaier, Synthesis of Deuterated and Protiated Triacylglycerides by Using 1,1'-Carbonyldiimidazole Activated Fatty Acids, European J Org Chem. (2023). https://doi.org/10.1002/ejoc.202300632.
[50] R. Schweins, K. Huber, Particle scattering factor of pearl necklace chains, in: Macromol Symp, 2004: pp. 25–42. https://doi.org/10.1002/masy.200450702.
[51] L. Onsager, The effects of shape on the interaction of colloidal particles, Ann N Y Acad Sci. 51 (1949) 627–659. https://doi.org/10.1111/j.1749-6632.1949.tb27296.x.
[52] L. Anghel, A. Rogachev, A. Kuklin, R.V. Erhan, β-Lactoglobulin associative interactions: a small-angle scattering study, European Biophysics Journal. 48 (2019) 285–295. https://doi.org/10.1007/s00249-019-01360-9.
[53] F. Zhang, F. Roosen-Runge, M.W.A. Skoda, R.M.J. Jacobs, M. Wolf, Ph. Callow, H. Frielinghaus, V. Pipich, S. Prévost, F. Schreiber, Hydration and interactions in protein solutions containing concentrated electrolytes studied by small-angle scattering, Physical Chemistry Chemical Physics. 14 (2012) 2483–2493.
[54] J. Kohlbrecher, W. Wagner, The new SANS instrument at the Swiss spallation source SINQ, J Appl Crystallogr. 33 (2000) 804–806. https://doi.org/10.1107/S0021889800099775.
[55] U. Keiderling, The new "BerSANS-PC" software for reduction and treatment of small angle neutron scattering data, Appl Phys A Mater Sci Process. 74 (2002) 1455–1457. https://doi.org/10.1007/s003390201561.
[56] S. Jaksch, V. Pipich, H. Frielinghaus, Multiple scattering and resolution effects in small-angle neutron scattering experiments calculated and corrected by the software packageMuScatt, J Appl Crystallogr. 54 (2021) 1580–1593. https://doi.org/10.1107/S1600576721009067.
[57] A. Brûlet, D. Lairez, A. Lapp, J.P. Cotton, Improvement of data treatment in small-angle neutron scattering, J Appl Crystallogr. 40 (2007) 165–177.
[58] R.J. Roe, Methods of X-Ray and Neutron Scattering in Polymer Science, Oxford University Press, 2000.
[59] M. Wagener, S. Förster, Fast calculation of scattering patterns using hypergeometric function algorithms, Sci Rep. 13 (2023) 780.
[60] V. Pipich, B. Wu, KWS-3 very small angle neutron scattering diffractometer: new opportunities for users. , In Proceedings of the Seventh Conference on Neutron Scattering-Programme and Abstracts. (2021).
[61] G. Baldini, S. Beretta, G. Chirico, H. Franz, E. Maccioni, P. Mariani, F. Spinozzi, Salt-induced association of β-lactoglobulin by light and X-ray scattering, Macromolecules. 32 (1999) 6128–6138. https://doi.org/10.1021/ma990709u.

[62] C. Cano-Sarmiento, D.I. Téllez-Medina, R. Viveros-Contreras, M. Cornejo-Mazón, C.Y. Figueroa-Hernández, E. García-Armenta, L. Alamilla-Beltrán, H.S. García, G.F. Gutiérrez-López, Zeta Potential of Food Matrices, Food Engineering Reviews. 10 (2018) 113–138. https://doi.org/10.1007/s12393-018-9176-z.

## Conflict of interest

The authors declare that they have no known competing financial interests or personal relationships that could have appeared to influence the work reported in this paper.

## Authors' contributions

- T. Heiden-Hecht: conceptualization, investigation, writing-original draft, visualization, writing-review & editing
- B. Wu, O. Holderer, K. Schwärzer and J. Kohlbrecher: methodology and investigation
- O. Holderer and H. Frielinghaus: writing-original draft, supervision, visualization, data analysis, writing - review & editing
- S. Förster: writing - review & editing

## Data availability statement

The SANS and SAXS data presented in this paper are available under Holderer, Olaf; Heiden-Hecht, Theresia; Frielinghaus, Henrich, 2023, "Beta Lactoglobulin emulsions SANS and SAXS data", https://doi.org/10.26165/JUELICH-DATA/PK8IS5

## List of figures:

**Fig.1:** SAXS curves of comparative concentration series of β-lg solubilized in distilled water (a) and β-lg stabilized emulsions (b) at pH 7. The intensities of the lowest curves are to scale, and the upper curves are scaled with factors of 10, 100, 1000, and 10,000 to improve visibility. SAXS data is fitted (black lines) with a *dimeric cylindrical model* for β-lg solubilized in distilled water (a) and for β-lg stabilized emulsions with protein concentrations above 0.25% (b), and with a *bicelle model* for β-lg stabilized emulsions with protein concentrations at or below 0.25% (b). The vertical lines indicate the position of the maxima, showing the protein internal structure either in solution (a), or at the oil/water interface in the emulsion (b). (color for web)

**Fig. 2:** SANS scattering patterns of β-lg stabilized emulsions at pH 7 with 0.25% (top) and 0.5% (bottom) protein concentration, with integrated background subtraction. The different contrasts refer to $D_2O$ and *d*-MCT-oil (protein contrast), $D_2O$ and *h*-MCT-oil (decorated droplet contrast), $H_2O/D_2O$ (60/40 ratio) and *d*-MCT-oil (droplet contrast), as well as $H_2O$ and *h*-MCT-oil (weak protein contrast). The dashed lines indicate the classical *Porod scattering* (red) and the interface coverage scattering (purple). The horizontal dotted line indicates the extrapolated protein scattering, i.e., its forward scattering. (color for web)

**Fig. 3**: Pair distance distribution functions and real space reconstruction from the corrected SANS scattering patterns of β-lg stabilized emulsions at pH 7 with 0.25% (black) and 0.50% (blue) protein concentration *(top),* and β-lg solubilized in $D_2O$ with 0.25% (black) and 0.50% (blue) protein concentration *(bottom)* in a Q-range from 0.03 to 0.3 $Å^{-1}$. (color for web)

**List of tables:**

**Table1:** List of neutron scattering length densities of used components. *For β-lg at all concentrations, we measured a density of $1 g/cm^3$; we assume also an equilibrium of deuterium and hydrogen of the otherwise hydrogenated protein with the surrounding and either hydrogenated, deuterated or mixed water phase.

**Table 2:** List of fit parameters of SAXS results according to used β-lg concentration. A dimeric cylindrical model ("2Cyl") was applied for β-lg solutions solubilized in water, and at higher protein concentrations in emulsions. A flat ellipsoidal model ("Bicelle") was used for emulsions with < 0.50 % β-lg.

Supporting Information

# New insights into protein stabilized emulsions captured via neutron and X-ray scattering: An approach with β-lactoglobulin at triacylglyceride-oil/water interfaces

Theresia Heiden-Hecht*[1], Baohu Wu[1], Kuno Schwärzer[2], Stephan Förster[1,2], Joachim Kohlbrecher[3], Olaf Holderer[1] and Henrich Frielinghaus[1]

[1] Jülich Centre for Neutron Science (JCNS) at Heinz Maier-Leibnitz Zentrum (MLZ), Forschungszentrum Jülich GmbH, Lichtenbergstr. 1, 85747 Garching, Germany
[2]Jülich Centre for Neutron Science (JCNS-1), Forschungszentrum Jülich GmbH, 52425 Jülich, Germany
[3]Paul Scherrer Institut, Villingen 5232, Switzerland
*Corresponding author: E-mail-address: t.heiden-hecht@fz-juelich.de, telephone-number: 004989158860841

## Models used for fitting the SAXS data in 3.1

The SAXS-data have been fitted with sasview 5.0.4 (http://www.sasview.org). The β-lg in solution has been described by a form factor comprising two domains with a radius of around 2 nm. The description with two spherical beads in contact with each other [S2] described well the higher-Q region and indicates that the protein is in a dimeric state in solution. A better description was achieved with two cylinders on the same axis separated by a thin layer of 0.1nm and an electron density changed by the same factor as the electron density between solvent and cylinders. The cylinders had approximately the same dimensions as the spheres-model. The interface decorated with β-lg has been fitted with the model "*core_shell_bicelle_elliptical*" [S3], which can account for some of the observed internal inhomogeneities compared to the protein in solution. The model was used with the following geometrical constraints: the core was set to the same electron density as the solvent, the core was surrounded by a rim of 0.5 nm thickness and faces of the elliptical cylindrical core also with 0.5 nm thickness. The electron density was changed by a factor of 1/6 for the rim and ½ for the faces of the bicelle. Only relative changes of the electron density have been considered here, no absolute scaling is used in the fits. The overall intensity (i.e. "scale" in sasview) of the model was used as a fit parameter to adjust the model.

The large axis of the ellipsoidal particle was stretched by 2 compared to the small axis. **Figure S1** shows the geometry of the models used for fitting the SAXS data. Both geometries have been made with the "*core_shell_bicelle_elliptical*"-model (https://www.sasview.org/docs/user/models/ core_shell_bicelle_elliptical.html) by choosing appropriate fixed parameters of the SLD.

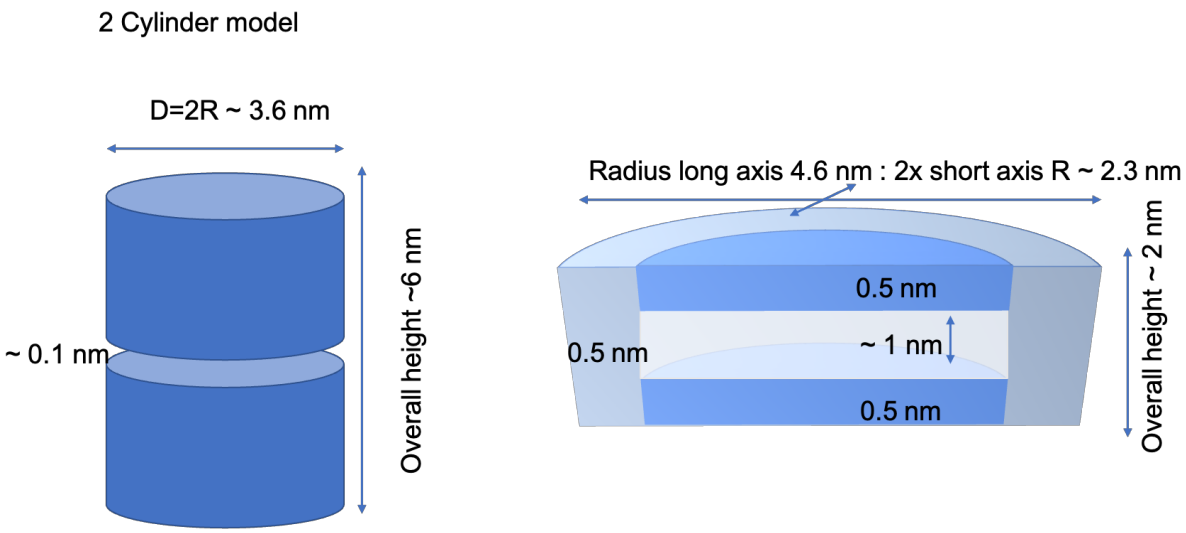


**Figure S1:** Geometrical models used for fitting the SAXS data. Left: Model for β-lg in water solutions. Right: Model for β-lg at oil/water interfaces.

## Bicelle modell

| **File generated by SasView** | | | | | | | | | | | | | | | | | |
|---|---|---|---|---|---|---|---|---|---|---|---|---|---|---|---|---|---|
| **Chi2** | Data | Scale | Scale (Err) | Back-ground ($cm^{-1}$) | Back-ground (Err, $cm^{-1}$) | Radius (Å) | Radius (Err, Å) | X_core (Å) | Thick_rim (Å) | Thick_face (Å) | Length (Å) | Length (Err, Å) | Sld_core ($10^{-6}$ Å$^{-2}$) | Sld_face ($10^{-6}$ Å$^{-2}$) | Sld_rim ($10^{-6}$ Å$^{-2}$) | Sld_solvent ($10^{-6}$ Å$^{-2}$) | Psi (-) |
| **1.8617** | Emulsion 0.05 % β-lg | 0.00158 | 2e-05 | 0.001034 | 3e-06 | 17.48 | 0.19 | 2 | 5 | 5 | 11.61 | 0.16 | 6 | 3 | 5 | 6 | 0 |
| **2.0743** | Emulsion 0.1 % β-lg | 0.00066 | 2e-05 | 0.001181 | 3e-06 | 17.87 | 0.47 | 2 | 5 | 5 | 11.88 | 0.39 | 6 | 3 | 5 | 6 | 0 |
| **2.7711** | Emulsion 0.2 % β-lg | 0.00471 | 2e-05 | 0.001100 | 3e-06 | 15.53 | 0.06 | 2 | 5 | 5 | 10.73 | 0.06 | 6 | 3 | 5 | 6 | 0 |
| **9.4522** | Solution 0.5 % β-lg | 0.00865 | 2e-05 | 0.001286 | 3e-06 | 17.10 | 0.04 | 2 | 5 | 5 | 9.24 | 0.03 | 6 | 3 | 5 | 6 | 0 |
| **18.094** | Solution 0.75 % β-lg | 0.01311 | 2e-05 | 0.001482 | 3e-06 | 17.55 | 0.03 | 2 | 5 | 5 | 9.12 | 0.02 | 6 | 3 | 5 | 6 | 0 |

## Two-cylinder modell

| **File generated by SasView** | | | | | | | | | | | | | | | | | |
|---|---|---|---|---|---|---|---|---|---|---|---|---|---|---|---|---|---|
| **Chi2** | Data | Scale | Scale (Err) | Background ($cm^{-1}$) | Background (Err, $cm^{-1}$) | Radius (Å) | Radius (Err, (Å) | X_core (Å) | Thick_rim (Å) | Thick_face (Å) | Thick_face (Err, (Å) | Length (Å) | Sld_core ($10^{-6}$ Å$^{-2}$) | Sld_face ($10^{-6}$ Å$^{-2}$) | Sld_rim ($10^{-6}$ Å$^{-2}$) | Sld_solvent ($10^{-6}$ Å$^{-2}$) | Psi (-) |

| | | | | | | | | | | | | | | | | | |
|---|---|---|---|---|---|---|---|---|---|---|---|---|---|---|---|---|---|
| **4.6309** | Emulsion 0.5 % β-lg | 0.001505 | 2e-06 | 0.00156 | 2E-03 | 17.83 | 0.02 | 1 | 1 | 35.70 | 0.09 | 2 | 0 | 3 | 6 | 6 | 0 |
| **5.1605** | Emulsion 0.75% β-lg | 0.002310 | 2e-06 | 0.001856 | 2e-06 | 17.98 | 0.01 | 1 | 1 | 34.87 | 0.06 | 2 | 0 | 3 | 6 | 6 | 0 |
| **2.0743** | Solution 0.05 % β-lg | 0.000118 | 3e-06 | 0.001033 | 4e-06 | 19.48 | 0.45 | 1 | 1 | 25.82 | 1.2 | 2 | 0 | 3 | 6 | 6 | 0 |
| **6.524** | Solution 0.1 % β-lg | 0.000265 | 2e-06 | 0.001268 | 2e-06 | 19.33 | 0.15 | 1 | 1 | 24.80 | 0.39 | 2 | 0 | 3 | 6 | 6 | 0 |
| **4.6676** | Solution 0.25 % β-lg | 0.000761 | 2e-06 | 0.001328 | 2e-06 | 18.36 | 0.05 | 1 | 1 | 24.72 | 0.14 | 2 | 0 | 3 | 6 | 6 | 0 |
| **3.1733** | Solution 0.5 % β-lg | 0.001565 | 2e-06 | 0.001213 | 2e-06 | 17.88 | 0.02 | 1 | 1 | 31.26 | 0.08 | 2 | 0 | 3 | 6 | 6 | 0 |
| **4.4164** | Solution 0.75 % β-lg | 0.002344 | 3e-06 | 0.001579 | 3e-06 | 17.96 | 0.02 | 1 | 1 | 30.41 | 0.06 | 2 | 0 | 3 | 6 | 6 | 0 |

**Table S0**: Full set of parameters with errors used to represent the two geometrical models in sasview for fitting the SAXS data. Since the scale has been used as a fitting parameter, the SLD values should only be seen as a relative value. The X-ray SLD of water and *h*-MCT oil is similar (of the order of 9 x $10^{-6}$ Å$^{-2}$, see e.g., the online calculator at https://www.ncnr.nist.gov/resources/activation/). The SLD of the protein deviates only slightly from this, providing a rather weak contrast, which is represented in the low factor of the scale parameter in the table above. It is significant enough to show the protein form factor as displayed in Fig 1 and the deviations induced by the interface (and represented in the models above), but for absolute values of the X-ray SLD difference, more detailed studies would be required.

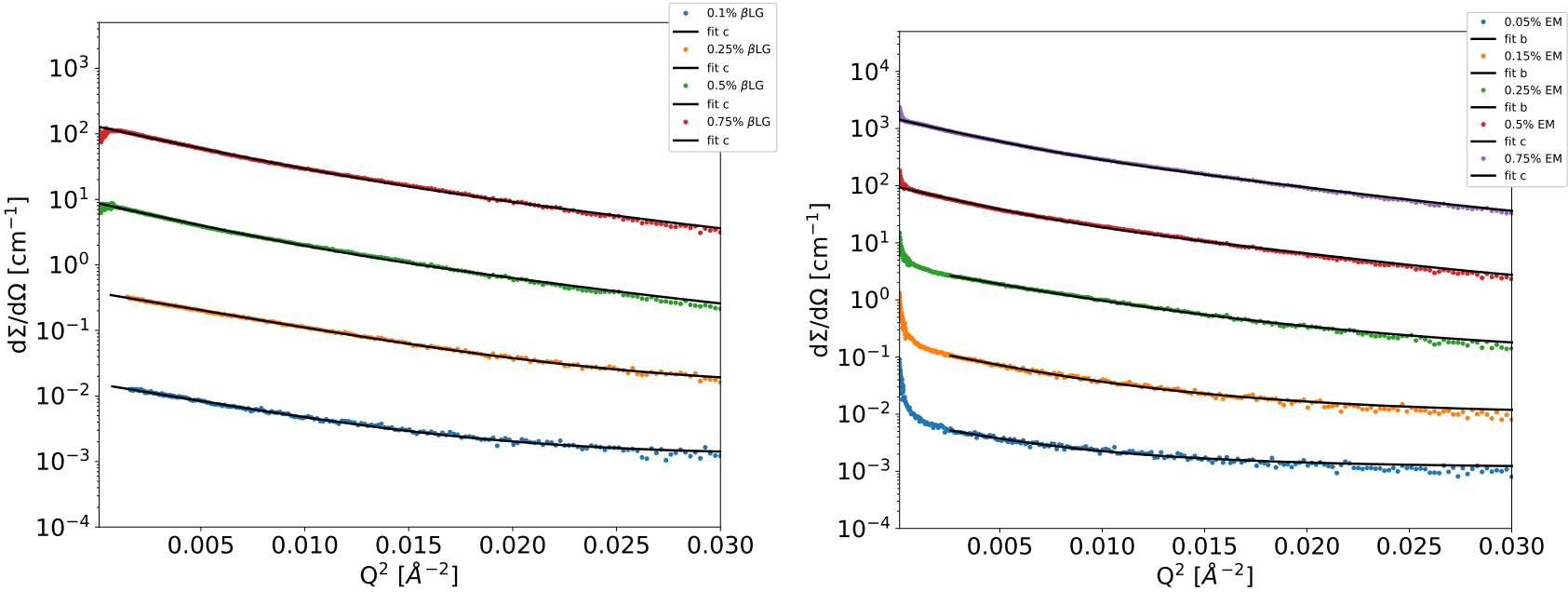


**Figure S2**: SAXS data in Guinier representation (ln(I(Q) vs $Q^2$) for pure β-lg (left) and the emulsions (right) with the model fits of the models described above. The "Guinier region" mentioned in the manuscript spans approximately up to Q2=0.01 Å$^{-2}$ (i.e. Q=0.1 Å$^{-1}$). The models are chosen to describe the data reasonably in the range up to Q=0.7 Å$^{-1}$.

**Models used for describing the SANS data in 3.2**

The SANS data has been described with the interfacial protein layer around the oil droplets, also called "protein shell", and the oil droplet size calculation has accounted the polydispersity of the oil droplet size distribution. The following paragraphs describe the calculation and derived formula in detail.

**The scattering of the protein shell**

We derive the scattering of a rather thin layer of proteins on a spherical oil droplet (for the protein contrast). The only contrast is between the hydrogenous proteins and the deuterated rest. The protein layer is assumed to appear homogenous for the considered $Q$-range. This means that we look at larger length scales than the single protein ($Q < 1/R_P$) and below the length scales of the whole oil droplet ($Q > 1/R_{oil}$). We then assume a radially symmetric protein shell around the droplet. The calibrated scattering intensity is then:

$$I_{\text{Interface}} = (\Delta\rho_P)^2 \phi_{\text{Ps}} \phi_S \frac{1}{V_S} \left( \int_0^{2\pi} d\varphi \int_{-1}^{1} d\cos\vartheta \int_{R_{\text{oil}}}^{R_{\text{oil}}+d_{PS}} r^2 \exp(iQr\cos\vartheta)\, dr \right)^2$$

$$= (\Delta\rho_P)^2 \phi_{\text{Ps}} \phi_S V_S \left( \frac{\sin(QR_{\text{oil}})}{QR_{\text{oil}}} \right)^2 \quad \rightarrow \quad \frac{1}{2} (\Delta\rho_P)^2 \phi_{\text{Ps}} \phi_S V_S \frac{1}{Q^2 R_{\text{oil}}^2} \tag{S1}$$

The first line derives from radial symmetry of the thin shell system. The contrast refers to the full compact protein and the solvents (oil and water). The concentration $\phi_{\text{Ps}}$ is the concentration of polymers within the thin shell of proteins at the oil surface. If it is not very compact it can be smaller than 1. The second concentration $\phi_{\text{S}}$ is the concentration of surfaces (shells) in the whole volume. It is assumed to be compact, and so

$$\frac{4\pi R_{\text{oil}}^2 d_{\text{Ps}}}{4\pi R_{\text{oil}}^3/3} = \frac{\phi_{\text{S}}}{\phi_{\text{oil}}} \quad \rightarrow \quad \phi_S = \frac{3 d_{\text{Ps}}}{R_{\text{oil}}} \phi_{\text{oil}} \tag{S2}$$

The volume of the shell is given by $V_{\text{S}} = 4\pi R_{\text{oil}}^2 d_{\text{Ps}}$. The last limit in eq. S1 is performed in the sense that heavy oscillations average out due to polydispersity and instrumental resolution. So, the scattering law becomes a simple power law. Combining all this together, we obtain finally:

$$I_{\text{Interface}} = 2\pi (\Delta\rho_P)^2 \phi_{\text{Ps}} \phi_{\text{oil}} \frac{3 d_{\text{Ps}}^2}{Q^2 R_{\text{oil}}} \tag{S3}$$

This formula is also used in the main text as eq. 2 (without polydispersity correction $C_{\text{interface}}$ derived further down).

**Polydispersity**

Because there are discrepancies between the droplet size obtained from the static light scattering particle sizer and the evaluation of the SANS *Porod scattering*, we decided to look at the influence of the polydispersity on the high-Q power laws (again between the droplet size and the protein size). We follow the considerations that were performed analytically in reference S1. For this we assumed the Schulz-Zimm distribution $h(R)$:

$$h(R) = \frac{(z+1)^{z+s+1} R^z}{R_0^{z+s+1} \Gamma(z+s+1)} \exp\left[-(z+1)\frac{R}{R_0}\right] \tag{S4}$$

The parameters are the mean radius $R_0$, the dimensionality $s = 2d = 6$, and the width of the distribution connected to the parameter $z$. The connection of $z$ to the standard deviation $\sigma$ is:

$$z = \frac{1-\sigma^z}{\sigma^z} \tag{S5}$$

When the distribution is applied to a form factor $f(R,Q)$, the following terms have to be considered to yield the polydisperse formfactor $P(Q)$ (please remember that the formfactor is normalized in this way that $f(R,Q\rightarrow 0) = 1$ and $P(Q\rightarrow 0) = 1$):

$$\langle P(Q)\rangle = \int_0^\infty f(R,Q) R^s h(R) dR \tag{S6}$$

The $R^s$ term arises from the scattering power of the single particle that is proportional to its squared volume in 3 dimensions. For the high-$Q$ power law of a compact sphere we arrive at the corrected *Porod scattering* (the oil droplet scattering):

$$\lim_{Q\rightarrow\infty} P_{\text{sphere}}(Q) = \frac{(z+s+1)^4}{(\mathrm{z+s})(\mathrm{z+s-1})(\mathrm{z+s-2})(\mathrm{z+s-3})} \frac{2\pi}{Q^4} \frac{A_{\text{oil}}}{V_{\text{oil}}^2} \tag{S7}$$

We use the droplet surface $A_{\text{oil}} = 4\pi R_{\text{oil}}^2$ and its volume $V_{\text{oil}} = \frac{4\pi}{3} R_{\text{oil}}^3$. We simply extract the correction factor:

$$C_{\text{Porod}} = \frac{(z+s+1)^4}{(\mathrm{z+s})(\mathrm{z+s-1})(\mathrm{z+s-2})(\mathrm{z+s-3})} \tag{S8}$$

The same exercise can be performed for thin disks, where the interesting scaling with $R^2$ is the same with our considerations of a thin shell around the oil droplet. So, the high-Q scattering of a polydisperse thin disk formfactor is:

$$\lim_{Q\to\infty} P_{\text{disk}}(Q) = \frac{(z+s+1)^2}{(\mathrm{z}+\mathrm{s})(\mathrm{z}+\mathrm{s}-1)} \frac{2\pi d_{\text{disk}}}{V_{\text{disk}}} \frac{1}{Q^2} \tag{S9}$$

Again, we have the disk volume $V_{\text{disk}} = \pi R_{\text{disk}}^2 d_{\text{disk}}$ and its area $A_{\text{disk}} = \pi R_{\text{disk}}^2$ . Please note, that here the dimensionality is $s = 2d = 4$. We extract the correction factor again:

$$C_{\text{interface}} = \frac{(z+s+1)^2}{(\mathrm{z}+\mathrm{s})(\mathrm{z}+\mathrm{s}-1)} \tag{S10}$$

The parameter z is determined by the 10% and 90% boundaries of the particle size distributions obtained from the static light scattering particle sizer. We calculated the ratio D90/D10 and matched the limited integral distribution (80%) to the z-value. In this sense, a reliable variance is obtained. We finally take the average values of $C_{Porod}$ = 2.64 ± 0.20 and $C_{interface}$ = 1.39 ± 0.04 in the main text.

**Table S1**: The parameters necessary to treat the polydispersity corrections of the SANS analysis.

| β-lg concentration | D10 (µm) | D50 (µm) | D90 (µm) | z | $C_{Porod}$ | $C_{interface}$ |
|---|---|---|---|---|---|---|
| 0.25% | 2.28 | 3.78 | 6.23 | 5.82 | 2.44 | 1.35 |
| 0.50% | 2.26 | 3.85 | 7.18 | 4.23 | 2.83 | 1.43 |

**SANS contrasts**

Neutron scattering allows for varying the contrast in the sample, by using fully or partly deuterated components. In the present case, *d*-MCT and $D_2O$ are the two components which can be varied. The main analysis referred to the case of the emulsion with fully deuterated solvents (*d*-MCT and $D_2O$), below the comparison to the *h*-MCT and $H_2O$ contrast case shows the usefulness for reducing incoherent background with deuterated components.

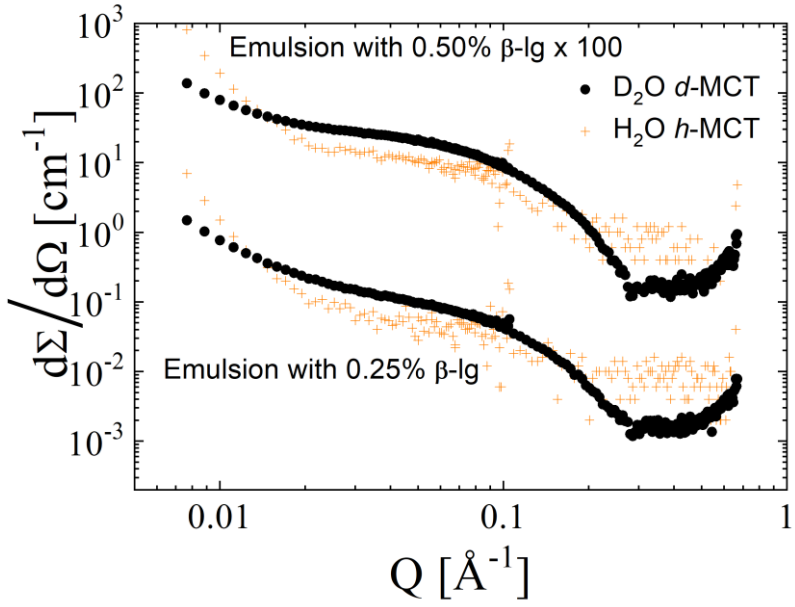


**Figure S3**: SANS data of emulsions with fully protonated and fully deuterated solvents (*h*-MCT and $H_2O$, *d*-MCT and $D_2O$) and protonated β-lg at the interface.

**References:**

[S1] M. Wagener, and S. Förster (2023). Fast calculation of scattering patterns using hypergeometric function algorithms. Scientific Reports, 13(1), 780. https://doi.org/10.1038/s41598-023-27558-8

[S2] R. Schweins, and K. Huber (2004). Particle Scattering Factor of Pearl Necklace Chains, Macromol. Symp. 211, 25-42. https://doi.org/10.1002/masy.200450702

[S3] L. Onsager (1949). The effects of shape on the interaction of colloidal particles. Ann. New York Acad. Sci., 51, 627-659. https://doi.org/10.1111/j.1749-6632.1949.tb27296.x

5: Figure 1

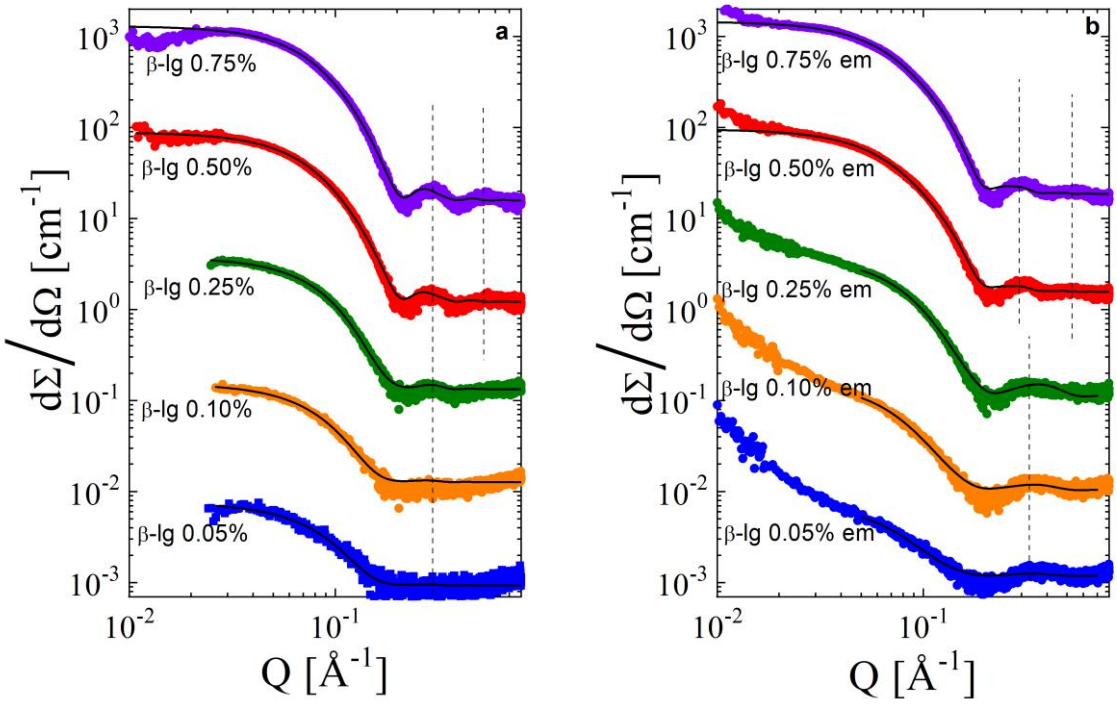
a
β-lg 0.75%
β-lg 0.50%
β-lg 0.25%
β-lg 0.10%
β-lg 0.05%
dΣ/dΩ [cm-1]
Q [Å-1]
b
β-lg 0.75% em
β-lg 0.50% em
β-lg 0.25% em
β-lg 0.10% em
β-lg 0.05% em
dΣ/dΩ [cm-1]
Q [Å-1]

5: Figure 2

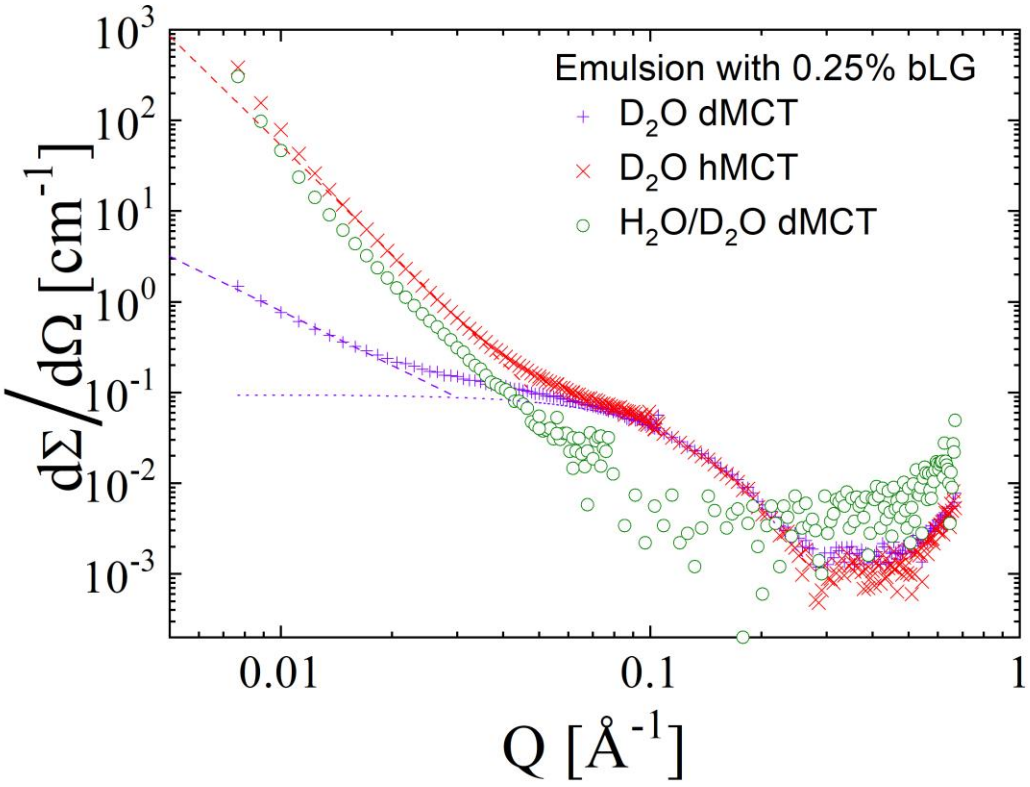
Emulsion with 0.25% bLG
D2O dMCT
D2O hMCT
H2O/D2O dMCT
dΣ/dΩ [cm-1]
Q [Å-1]
10^3
10^2
10^1
10^0
10^-1
10^-2
10^-3
0.01
0.1
1

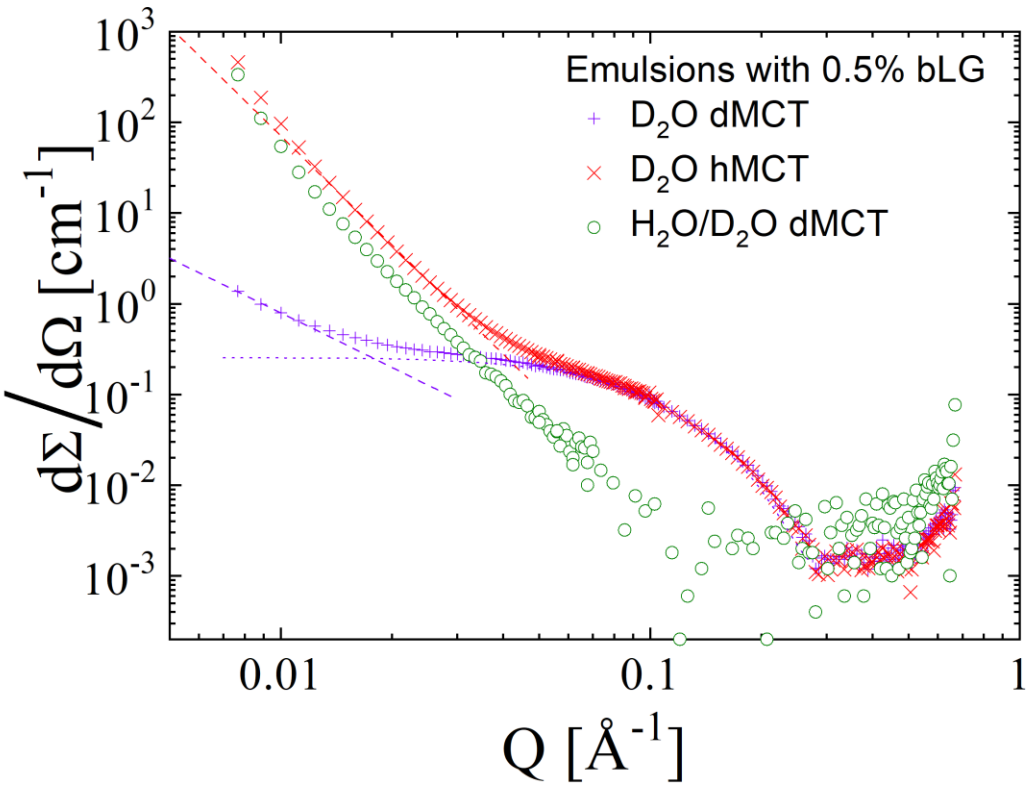
Emulsions with 0.5% bLG
D2O dMCT
D2O hMCT
H2O/D2O dMCT
dΣ/dΩ [cm-1]
Q [Å-1]
10^3
10^2
10^1
10^0
10^-1
10^-2
10^-3
0.01
0.1
1

5: Figure3

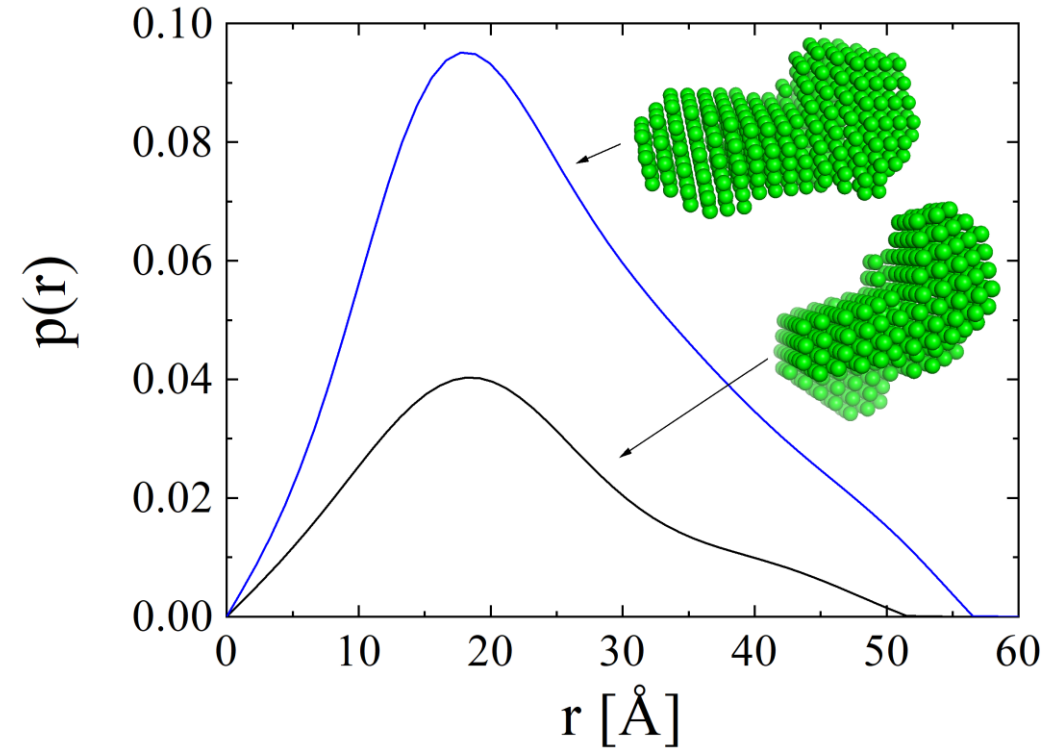
0.10
0.08
0.06
0.04
0.02
0.00
p(r)
0
10
20
30
40
50
60
r [Å]

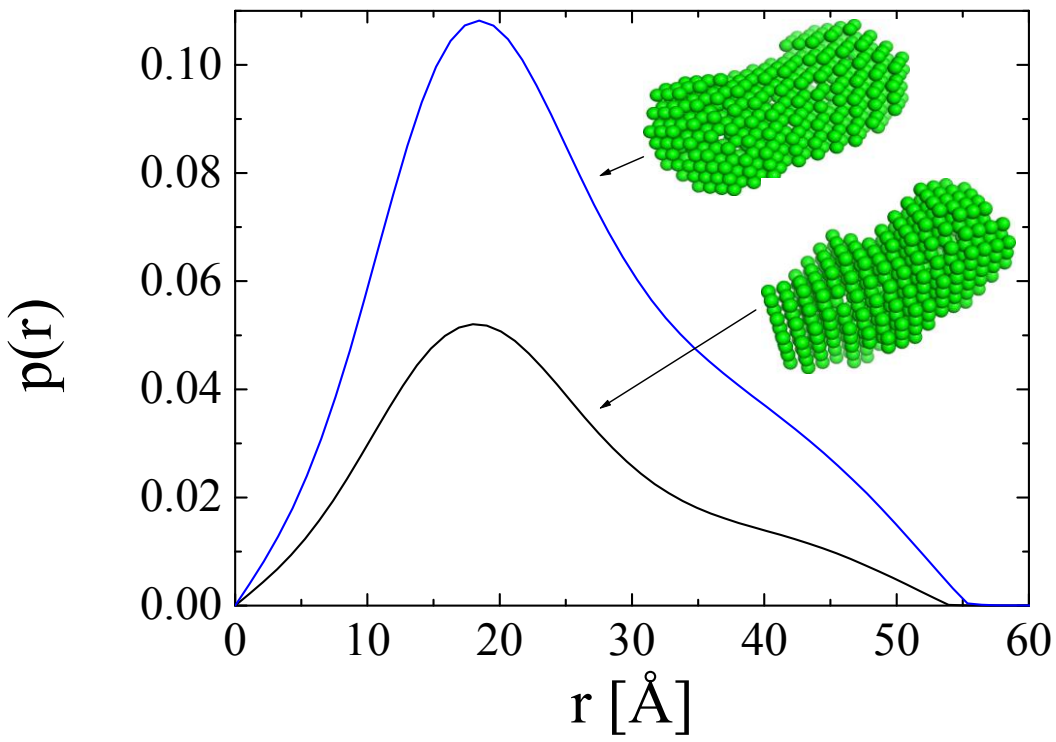
0.10
0.08
0.06
0.04
0.02
0.00
p(r)
0
10
20
30
40
50
60
r [Å]

**Table1:** List of neutron scattering length densities of used components. *For β-lg at all concentrations, we measured a density of 1g/cm$^3$; we assume also an equilibrium of deuterium and hydrogen of the otherwise hydrogenated protein with the surrounding and either hydrogenated, deuterated or mixed water phase.

| | SLD [$10^{-6}$ Å$^{-2}$] | |
|---|---|---|
| Component | hydrogenated | deuterated |
| Water | -0.56 | 6.36 |
| MCT-Oil | 0.28 | 6.75 |
| β-lg* | 1.27 | 2.19 |

**Table 2:** List of fit parameters of SAXS results according to used β-lg concentration. A dimeric cylindrical model ("2Cyl") was applied for β-lg solutions solubilized in water, and at higher protein concentrations in emulsions. A flat ellipsoidal model ("Bicelle") was used for emulsions with < 0.5 % β-lg.

| | β-lg concentration | Chi2 best model | Chi2 Bicelle model | Best model | Radius (Å) | err.Radius (Å) | Ellipse | Overall height (Å) | err Overall height (Å) |
|---|---|---|---|---|---|---|---|---|---|
| **Solution** | 0.05 | 2.9002 | | 2Cyl | 19.5 | 0.45 | 1 | 52.6 | 1.19 |
| | 0.10 | 6.5240 | | 2Cyl | 19.3 | 0.15 | 1 | 51.6 | 0.39 |
| | 0.25 | 4.6676 | | 2Cyl | 18.4 | 0.05 | 1 | 51.4 | 0.14 |
| | 0.50 | 3.1733 | ´ | 2Cyl | 17.9 | 0.02 | 1 | 64.5 | 0.08 |
| | 0.75 | 4.4164 | ´ | 2Cyl | 18.0 | 0.02 | 1 | 62.8 | 0.06 |
| **Emulsion** | 0.05 | 1.8617 | 1.8617 | Bicelle | 22.5 | 0.20 | 2 | 21.6 | 0.16 |
| | 0.10 | 2.0743 | 2.0743 | Bicelle | 22.9 | 0.47 | 2 | 21.9 | 0.39 |
| | 0.25 | 2.7711 | 2.7711 | Bicelle | 20.5 | 0.06 | 2 | 20.7 | 0.06 |
| | 0.50 | 4.6309 | 9.4522 | 2Cyl | 17.8 | 0.02 | 1 | 73.4 | 0.09 |
| | 0.75 | 5.1605 | 18.094 | 2Cyl | 18.0 | 0.01 | 1 | 71.7 | 0.06 |

**Authors' contributions**

- T. Heiden-Hecht: conceptualization, investigation, writing-original draft, visualization, writing-review & editing
- B. Wu, O. Holderer, K. Schwärzer and J. Kohlbrecher: methodology and investigation
- O. Holderer and H. Frielinghaus: writing-original draft, supervision, visualization, data analysis, writing - review & editing
- S. Förster: writing - review & editing